Spectroscopy 26 (2011) 213–229
DOI 10.3233/SPE-2011-0543
IOS Press

Structural characterization of recombinant bovine Goα by spectroscopy and homology modeling

Pinar Mega Tiber [a,*], Oya Orun [a,*], Cevdet Nacar [a], Ugur Osman Sezerman [b], Feride Severcan [c], Mete Severcan [d], André Matagne [e] and Beki Kan [a,f,**]

[a] *Department of Biophysics, Marmara University School of Medicine, Istanbul, Turkey*
[b] *Biological Sciences and Bioengineering, Sabanci University, Orhanli, Tuzla, Istanbul, Turkey*
[c] *Department of Biology, Middle East Technical University, Ankara, Turkey*
[d] *Department of Electrical and Electronics Engineering, Middle East Technical University, Ankara, Turkey*
[e] *Laboratory of Enzymology and Protein Folding, Centre for Protein Engineering, Institut de Chimie B6, University of Liège, Liège, Belgium*
[f] *Department of Biophysics, School of Medicine, Acibadem University, Istanbul, Turkey*

Abstract. Go, a member of heterotrimeric guanine nucleotide-binding proteins, is the most abundant form of G protein in the central and peripheral nervous systems. Goα has a significant role in neuronal development and function but its signal transduction mechanism remains to be clarified.

In this study, the bovine Goα subunit was overexpressed and purified into homogeneity. Its activity was studied using [^{35}S] GTPγS binding, intrinsic fluorescence and BODIPY assays. The secondary structure was determined by both FTIR and CD spectroscopy as 42.3% α-helix, 13.4% β-sheet and 24.3% β-turn. A theoretical structure model was constructed. The structure from homology modeling is in very good agreement with the crystal structure of mouse Goα subunit except for the loop between αB–αC helices. This model was docked to the mouse RGS16 molecule. T117 on the αB–αC loop of Goα interacted with K172 on RGS16 as opposed to the T117 and K164 interaction in mouse.

Keywords: Goα protein, FTIR spectroscopy, circular dichroism, homology modeling

Abbreviations

FTIR	Fourier transform infrared;
GRIN1	G protein-regulated inducer of neurite outgrowth 1;
RGS	regulators of G-protein signaling;
β-Me	β-mercaptoethanol;
IPTG	isopropyl β-D-thiogalactoside;
Ni-NTA	nickel-nitrilotriacetic acid;
ATR	attenuated total reflectance;

[*] These authors contributed equally to this work.
[**] Corresponding author: Beki Kan, Department of Biophysics, School of Medicine, Acibadem University, Gulsuyu Mah. Fevzi Cakmak Cad., Divan Sok. No. 1, Maltepe 34848, Istanbul, Turkey. Tel.: +90 216 458 08 25; Fax: +90 216 589 84 85; E-mails: beki.kan@acibadem.edu.tr, bekimkan@yahoo.com.

PBS phosphate-buffered saline;
DCT discrete cosine transforms;
CD circular dichroism;
GEF guanine nucleotide exchange factor;
GAP GTPase accelerating protein.

1. Introduction

Heterotrimeric guanine nucleotide-binding proteins (G proteins) transduce a variety of signals from a large number of heptahelical receptors at the cell surface to intracellular effectors [13,18]. G proteins are composed of an α-subunit that binds and hydrolyzes GTP and of β- and γ-subunits that form a nondissociable complex (G$\beta\gamma$). To date, 21 different Gα-, 6 Gβ- and 11 Gγ-subunits have been identified. Gα subunits have been classified into four families on the basis of sequence alignments: Gαs, Gαi/o, Gαq/11 and Gα12/13 [42]. Their molecular mass is comprised between 39 and 52 kDa [18,33]. When an agonist-activated receptor stimulates G proteins, the α-subunit exchanges GDP for GTP (Gα.GTP). Both Gα.GTP and G$\beta\gamma$ can initiate a wide range of downstream signaling events. The response is terminated when the Gα-subunit hydrolyzes GTP to GDP and re-associates with the G$\beta\gamma$-subunit to enter a new cycle.

Go, a member of the Gi/o family, is the most abundant G protein expressed in the brain and central nervous system [45]. A group of common receptors, including α2 adrenergic, D2 dopamine, opioid, 5HT1, somatostatin and the muscarinic M_2 and M_4 receptors activate Gi and Go proteins [47]. In contrast to other G proteins, most functions of Go appear to be primarily mediated by a common pool of G$\beta\gamma$ dimers [5], but the effectors directly regulated by Goα remain to be identified. So far, one Goα effector molecule, G protein-regulated inducer of neurite outgrowth 1 (GRIN1), has been identified in brain. GRIN1 colocalizes with Goα in the growth cones of neuronal cells and promotes neurite extension in Neuro2a cells when coexpressed with constitutively active mutant GoαQ205L [4,31]. Goα has been shown to be colocalized with the metabotropic glutamate receptor 6 (mGluR6) in ON bipolar dendrites [46]. Although the mechanisms of signal transduction of Goα are essentially unclear, the possible link of Goα-GRIN1 pathway in neurite outgrowth [31], the implicated role of Goα in neuroendocrine tumors [8,24] and in Alzheimer's disease [32] place Goα as an important target for drugs.

To date, crystal structures of various G-proteins have been reported and many aspects of their structure have been well documented [38]. These studies have provided a comprehensive explanation of the activation cycle and receptor–G-protein interactions. The structure of Goα, however, was not determined until recently. The first crystal structure of Goα in the GTP hydrolytic transition state, in complex with RGS16, was obtained by Slep et al. [43].

The regulators of G-protein signaling (RGS) proteins help to accelerate GTPase activity by stabilizing the transition state of hydrolysis, and thereby play an important role in regulation. The mouse Goα.RGS16 complex, Goα.GDP.AlF_4.RGS16, displays a clear structural homology with Gi1α and Gi1/tα structures in their transition state. Comparison with the Giα.RGS16 structure also indicated that the major conformational differences are found in the helical domain of Goα, mainly in the αB helix and in the loop connecting αB and αC helices. Determining these structural differences of Goα with other members of the Gi/o protein family will provide clues on its preference in the central nervous system and the specific determinants in receptor and effector coupling.

The structure of a protein can be determined more precisely by X-ray crystallography; however, there are some disadvantages of this technique. The most important limitation of X-ray crystallography is

that the analysis of X-ray diffraction data presents a static picture of a protein structure. Therefore, the structure of a protein in crystal form may not relate to its structure in solution. One can study proteins in their natural aqueous environment using Nuclear Magnetic Resonance (NMR) spectroscopy, but this high resolution technique is limited to the analysis of small proteins. The drawbacks of these high resolution techniques prompted the development of low resolution techniques such as Fourier transform infrared (FTIR) and circular dichroism (CD) spectroscopy.

In the present study, the complete bovine Goα protein subunit was purified to homogeneity and its activity was verified by different assays. Both FTIR and CD spectroscopy were used for estimating the secondary structural content of the protein in solution and finally, a plausible structure of the loop region, a putative effector engagement site, was constructed by using homology modeling. This study showed that the topology of Goα in solution is similar to that in its crystal state and further confirmed the possible role of its loop region in effector interactions.

2. Materials and methods

2.1. Materials

The pT7/NdeI/Goα vector was a kind gift of Dr. Joel Moss [23]. The anti Goα monoclonal antibody and alkaline phosphatase-conjugated goat anti-mouse IgG were purchased from Calbiochem (San Diego, CA, USA). [^{35}S] GTPγS was from Amersham Biosciences (Uppsala, Sweden). Electrophoresis reagents were purchased from Sigma-Aldrich (St. Louis, MO, USA). The protease inhibitor cocktail was from Roche Diagnostics (Mannheim, Germany). BODIPY FL-GTPγS was purchased from Molecular Probes Inc. (Eugene, OR, USA). Chromatography resins were obtained from the following sources: Ni-NTA from Qiagen (Valencia, CA, USA), Sephadex G-100 from Sigma-Aldrich and Mono Q 5/5 from Amersham Biosciences. Mouse anti-Goα monoclonal antibody and alkaline phosphatase-conjugated goat anti-mouse antibody were from Chemicon International (Temecula, CA, USA).

2.2. Plasmid construction

cDNA encoding the bovine brain Goα subunit was amplified by PCR from the template pT7/NdeI/Goα, using the following primers: 5′-GCATGCGAGCTCATCGGATGTACT-3′ (sense), 5′-GACCCGA AGCTTCTAGTACAAGCC-3′ (antisense). The products were double-digested using SacI and HindIII restriction enzymes. The gel-purified, restriction-digested PCR products were subcloned into pQE-80 vector (Qiagen, Valencia, CA, USA). The construct was verified using an automated sequencer.

2.3. Expression and purification of recombinant protein

Goα-His$_6$ was expressed in the *E. coli* TOP10 cell line (Invitrogen, Carlsbad, CA, USA) by induction with 1 mM isopropyl β-D-thiogalactoside (IPTG) at 25°C for 16 h. Cells were harvested and resuspended in lysis buffer containing 50 mM Tris-HCl pH 8.0, 20 mM β-mercaptoethanol (β-Me), 0.1 mM PMSF, and protease inhibitor cocktail (1 tablet/50 ml). Lysozyme, DNase I and $MgSO_4$ were added to final concentrations of 0.2 mg/ml, 20 U/μl or 2 μg/μl, and 5 mM, respectively. Following sonication for 5×30 s on ice, the lysate was clarified by centrifugation at $4000 \times g$ at 4°C for 1 h. The supernatant was applied to a 3 ml nickel-nitrilotriacetic acid (Ni-NTA) agarose column equilibrated with a buffer containing 50 mM Tris-HCl pH 8.0, 20 mM β-Me, 0.1 mM PMSF, and 100 mM NaCl. The column

was washed with the same buffer containing 500 mM NaCl and 10 mM imidazole. Goα-His_6 was eluted with a buffer containing 50 mM Tris-HCl pH 8.0, 20 mM β-Me, 0.1 mM PMSF, and 10% glycerol, with a series of increasing step gradients of imidazole in the range of 25–150 mM. Fractions containing Goα were pooled, adjusted to 1.2 M $(NH_4)_2SO_4$ and 50 μM GDP. Sephadex G-100 size exclusion and Mono Q anion exchange chromatography were used for further purification. The Sephadex G-100 column (1 × 50 cm) was equilibrated with a buffer containing 50 mM Tris-HCl pH 8.0 and 100 mM KCl. An Acta Prime FPLC system was used to load on a HiTrap Q HP, 5 ml, column (GE Healthcare, Piscataway, NJ, USA) equilibrated with 50 mM Tris-HCl pH 8.0. Purification was carried out using 0–700 mM NaCl gradient in 50 mM Tris-HCl pH 8.0 over a volume of 30 ml with a flow rate 3 ml/min and 0.5 ml fractions were collected.

2.4. GTPγS binding assay

GTP binding efficiencies of peak fractions from different stages of purification were determined using a nonhydrolyzable analog of GTP, [^{35}S] GTPγS. Each assay tube contained 25 mM sodium HEPES pH 8.0, 30 mM $MgCl_2$, 100 mM NaCl, 1 mM sodium EDTA, 1 mM DTT (dithiothreitol), 0.1% Lubrol and 1 μM [^{35}S] GTPγS (3×10^5 cpm/min; 1000 Ci/mMol). Tubes were incubated for 1 h at 30°C, and binding was terminated by the addition of 3 ml of ice-cold wash buffer (20 mM Tris HCl pH 8.0, 100 mM NaCl, and 25 mM $MgCl_2$) followed by rapid filtration through 25 mm HA WP nitrocellulose filters (Millipore, Bedford, MA, USA), under vacuum. Filters were rinsed three times with wash buffer again and counted in a Beckman liquid scintillation counter.

2.5. Intrinsic tryptophan fluorescence of Goα

Fluorescence spectra were recorded on a Photon Technology International spectrophotometer, with excitation at 290 nm and emission at 346 nm. Measurements were made at 20°C in 50 mM sodium HEPES, pH 8.0, in the presence of 1 mM sodium EDTA, 1 mM DTT and 0.1% (v/v) lubrol (buffer A). The sample, 400 μl in a 5 × 5 mm quartz cell, was continuously stirred. The background signal obtained with buffer alone was subtracted from all data.

2.6. BODIPY FL/GTPγS-Goα

The assay using BODIPY FL/GTPγS as a probe was carried out in buffer B containing 10 mM sodium HEPES pH 8.0, 1 mM EDTA, and 10 mM $MgSO_4$. Fluorescence of the probe (50 mM) alone was measured in buffer B for 2 min and binding was initiated by adding 400 nM of Goα. The fluorescence signal was recorded for 35 min. Subsequent to binding, dissociation was initiated with the addition of 20 μM GTPγS and an additional 30 min record was obtained. Excitation was at 485 nm and total fluorescence emission was measured above 530 nm, using a cut off pass filter [3,29].

2.7. Western blot analysis

Protein fractions from various stages in the purification (∼50 μg protein) were resolved by SDS-PAGE and electrophoretically transferred to nitrocellulose sheets. Western blots were processed for immunoreactions with mouse monoclonal anti G protein Goα antibody. Immune reactive proteins were visualized using alkaline phosphatase-conjugated secondary antibodies by a colorimetric reaction.

2.8. ATR–FTIR spectroscopy, spectral acquisition and data processing

Infrared spectra were obtained using the one-bounce ATR (Attenuated Total Reflectance) mode in a Spectrum 100 Spectrometer (Perkin Elmer, Norwalk, CT, USA), equipped with a Universal ATR accessory. The protein (5 mg/ml) in phosphate-buffered saline (PBS, 137 mM NaCl, 2.7 mM KCl, 10 mM Na_2HPO_4, 1.76 mM KH_2PO_4 pH 7.4) supplemented with 50 μM GDP, was placed on a Diamond/ZnSe crystal plate. The interfering spectrum of air was recorded as background and subtracted automatically by using appropriate software (Spectrum 100 software). The spectra were recorded in the 3000–1000 cm^{-1} region at room temperature. A total of 300 scans were taken for each interferogram at 4 cm^{-1} resolution. The spectrum of GDP in buffer recorded at identical conditions, at the concentration that was used in protein isolation, was digitally subtracted from the protein spectrum to give a straight baseline between 2000 and 1800 cm^{-1}. The protein spectrum was also taken directly by scanning GDP in buffer as a background and identical spectra were obtained. The second derivative spectral analysis was only used to verify and assign the position of the overlapping components of the Amide I band using the same software. The derivatives give the number and positions, as well as an estimation of the bandwidth and intensity of the bands making up the Amide I region; however, for precise determination of secondary structure content only the Amide I absorbance band was used.

2.9. Protein secondary structure composition determination based on FTIR data

Protein secondary structure composition was predicted through the software developed by Severcan et al. [41]. To achieve this, infrared absorption values measured at many points (around 100) in 1600–1700 cm^{-1} spectral region, which corresponds to Amide I band, are used. Neural networks are initially trained using a data set containing FTIR spectra of a number of water-soluble proteins recorded in water. The secondary structures of these proteins are known from X-ray crystallographic analysis. In order to improve the training of neural networks, the size of the data set can be increased by interpolating the available FTIR spectra. Before starting the training procedure, FTIR spectra of Amide I band are normalized and then their discrete cosine transforms (DCT) are obtained. DCT is a good approximation by which it is possible to represent a signal with the least number of coefficients for a specified amount of error. Bayesian regulation is used to train the neural networks. Bayesian regulation minimizes a combination of squared errors and weights and determines the correct combination to produce a neural network, which generalizes well [41].

2.10. Circular dichroism measurements

Circular dichroism (CD) measurements in the far UV region were performed at 20°C, with a Jasco J-810 spectropolarimeter (Jasco, Japan), using protein concentrations of 0.04–0.08 mg/ml (0.95–1.9 μM) and a 0.1 cm cell path length. The buffer used was PBS supplemented with 50 μM GDP. Spectra were acquired at a scan speed of 10 $nm \cdot min^{-1}$, with a 0.1 nm data pitch, using a 1 nm bandwidth and a 4 s response time. The spectra were averaged after five accumulations and corrected by subtraction of the buffer spectrum obtained under the same conditions. Protein concentrations were determined by absorbance measurements at 280 nm, using a molecular extinction coefficient of 30,370 $M^{-1} \cdot cm^{-1}$, calculated using the method of Pace et al. [34]. Ellipticity measurements in mdeg were converted in molar mean residue ellipticity, by multiplying the protein concentration by the number of amino acid residues (MRW = 113.22). The CD spectra were analyzed using CONTIN, CDSSTR and SELCON programs in the CDPro secondary structure prediction package [44]. Deconvolution of the CD spectra

was also performed using the K2d program provided in DICHROWEB [48,49], a facility of the BBSRC Centre for Protein and Membrane Structure and Dynamics.

2.11. Homology modeling of bovine Goα

The tertiary structure of bovine Goα was obtained by homology modeling. Proteins of known structure, displaying similarities with the bovine sequence, were identified using a BLAST search with default parameters. Two sequences [PDB IDs: *1cip*, *1bof*] with a similarity greater than 70% with the Goα-bovine sequence were found. Their tertiary structures have been determined by X-ray crystallography, with resolutions of 1.5 and 2.2 Å, respectively [6,7]. The Goα-bovine sequence was aligned with these two Giα protein sequences using ClustalX [26] and this was used as a basis for homology modeling (Table 1). 1cip structure was used as the template on the basis of a better sequence alignment, except

Table 1

The alignment of Goα-bovine sequence with two Giα protein sequences (*1cipA, 1bof*). (Colors are visible in the online version of the article; http://dx.doi.org/10.3233/SPE-2011-0543)

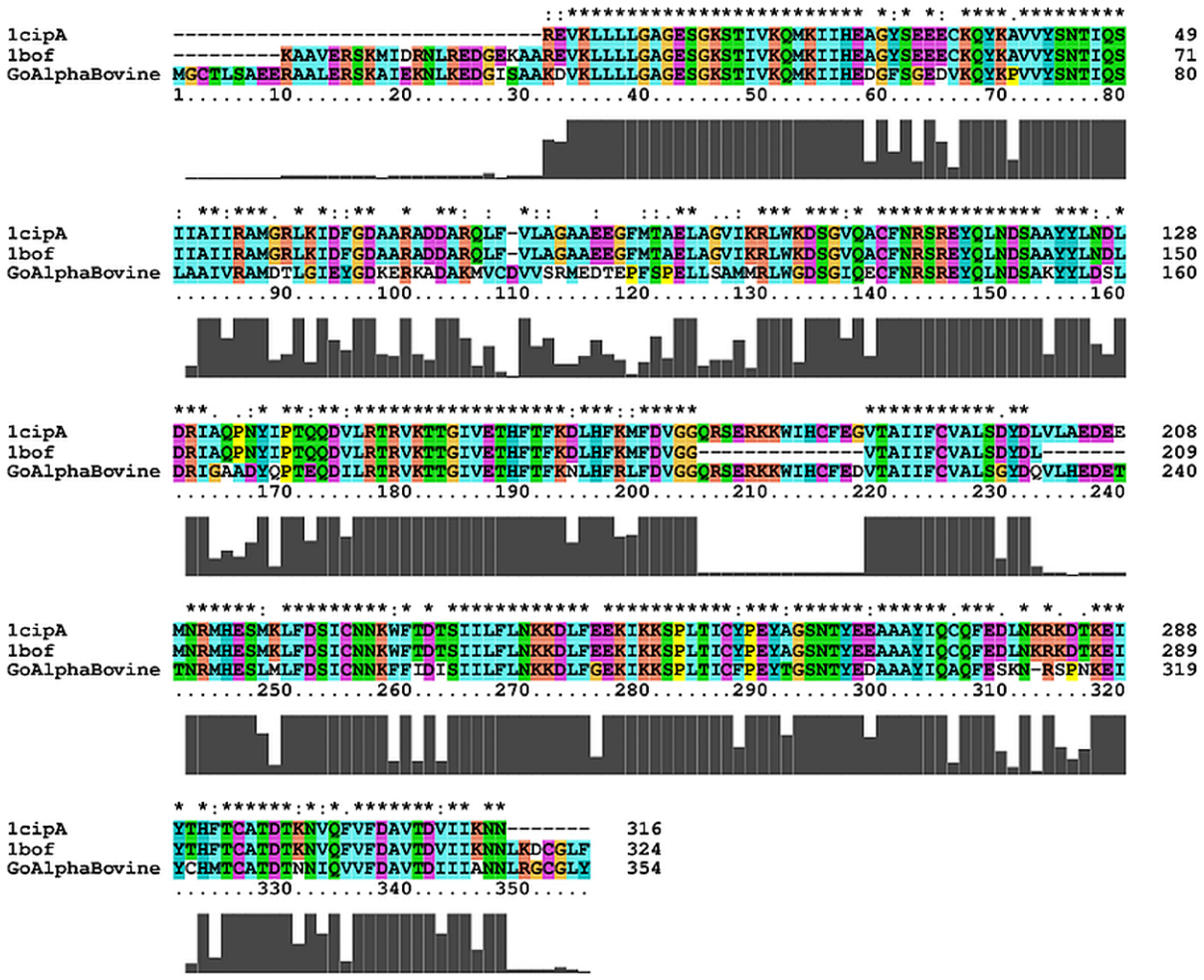

for the first 22 and the last 7 residues, for which 1bof proved to fit better. Because the interactions between the atoms of Goα residues and GDP-Mg^{2+} are well known, 19 distance restraints corresponding to ligand interactions derived from the structure of ras protein [35] which has high sequence similarity to the GTPase domain of Goα (bovine) were kept constant for the model. As can be seen from Table 1, even though the overall sequence similarity is very high, the similarity between residues 108 to 130 is low. Since residues 115 to 121 correspond to a loop region, which is solvent accessible in the template, we built several models for this loop and selected the energetically most favorable model. Homology modeling and loop structure refinements were performed using MODELLER (v9.1) software [11, 39], whereas energy minimization of the structure was done by molecular dynamics simulation, using "NAMD (v2.6)/VMD (1.8.7)/CHARMM force field" for 1 ns [22,37]. Protein structures were visualized by the CHIMERA (v1.5.3) software [36]. Docking of the modeled bovine Goα to mouse RGS16 molecule was done by using HADDOCK package [9,10]. Two molecules were positioned 150 Å apart from each other and applying random rotations and translations the molecules were docked to each other. During docking residues 181–183, 208–211 and 117 from Goα (bovine) and residues 90, 130 and 172 from the 3CK7-D structure were selected for potential interacting residues to limit the search space. The finalized complex was obtained after rigid body energy minimizations using rotations and translations.

3. Results

3.1. Expression, purification and characterization of Goα

Bovine brain Goα fused to the His_6-tagged-pQE-80 vector was expressed and purified as described under Materials and methods. Different IPTG concentrations and temperatures were assayed to induce overexpression of Goα. Optimal soluble yields for Goα were obtained after induction overnight at 25°C with 1 mM IPTG. Goα-His_6 was first purified through Ni-NTA agarose column and then subjected to size-exclusion chromatography on a Sephadex G-100 column. The GTPγS binding activity was enhanced 25-fold (Table 2); however, only high molecular weight contaminants were removed after G-100 chromatography. For further purification, the fractions containing the protein of interest were pooled, dialyzed and loaded on a HiTrap Q HP column. Purity and characterization of protein were verified with SDS-PAGE, Western blot and GTPγS binding analyses after each purification step (data not shown). An 81-fold enrichment was achieved at the end of the three-step purification procedure and the yield from 4 l culture was 1.06 mg, as indicated in Table 2.

Table 2

Yields and specific activities of fractions through different purification stages. Specific activity was determined by [^{35}S] GTPγS binding

Purification steps	Total protein (mg)	Total activity (pmol)	Specific activity (pmol/mg)	Purification (fold)	Yield (%)
Lysate	600	195	0.32	1	100
Cytoplasmic	180	62	0.34	1.06	31.8
Ni-NTA	40	33.02	0.82	2.56	16.9
G-100	1.53	30.92	20.6	64.4	15.8
HiTrap Q HP	1.06	27.7	26.1	81.5	14.2

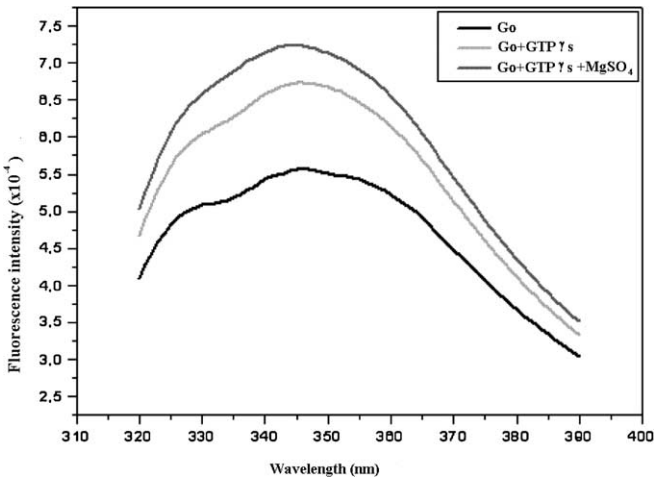

Fig. 1. Intrinsic tryptophan fluorescence of Goα. Goα (400 nM) was incubated for 30 min at 20°C in either buffer A with 1 μM GTPγS or 1 μM GTPγS and 10 mM $MgSO_4$. The fluorescence emission spectrum was observed with an excitation wavelength of 290 nm. The emission spectrum of each sample was recorded between 300 and 410 nm.

3.2. Intrinsic tryptophan fluorescence of Goα

Goα contains two tryptophan residues, Trp132 and Trp212 and its fluorescence intensity increases when GTP binds. Trp 212 which is in close proximity to the nucleotide-binding pocket is thought to be responsible for this fluorescence signal [21]. The fluorescence of Goα in buffer A displayed an emission maximum at 346 nm, characteristic of partially solvent accessible tryptophan. The fluorescence intensity (Fig. 1) increased by about 20% in the presence of 1 μM GTPγS and this was further enhanced (up to 31%) upon addition of Mg^{2+}.

3.3. The kinetics of GTP and GTPγS binding and GTP hydrolysis

The kinetics of the GTP- and GTPγS-induced enhancement of tryptophan fluorescence emission were compared. The fluorescence emission was monitored at 1 min intervals at 20°C. When 1 μM GTPγS was added to a 400 nM Goα solution, there was a slow, exponential increase in the fluorescence intensity. At steady state, which was achieved in 12 min, the fluorescence intensity exceeded the baseline value by 17.6%. The subsequent addition of 10 mM Mg^{2+} caused a rapid additional increase in emission of 12.5%, followed by a fast decay to a level that exceeded the steady state value by 3% and the GDP-bound form of the protein by approximately 20% (Fig. 2(A)). The binding rate of Goα to GTPγS was found to be 0.36 ± 0.05 min^{-1} (fit to the equation $y = a(1 - e^{-kt})$ after subtracting steady-state fluorescence of Goα, using nonlinear regression curve fit, one phase exponential association in GraphPad Prism Software, V.4.0). The change in fluorescence emission of Goα, upon GTP binding, was monitored at 340 nm, with 10 μM GTP and 10 mM Mg^{2+}, added to the mixture after 4 and 16 min, respectively. Upon addition of GTP, immediate decrease in the fluorescence intensity was observed, due to absorbance of the guanine nucleotide. GTP binding to Goα caused a linear increase in the fluorescence intensity (Fig. 2(B)). Addition of Mg^{2+} after steady state was reached led to a steep increase in intensity; followed by a rapid decrease (2.4 min^{-1}, fit to the equation $y = ae^{-kt}$, using nonlinear regression curve fit, one phase exponential decay in GraphPad Prism Software, V.4.0) due to GTP hydrolysis, down to ∼15%

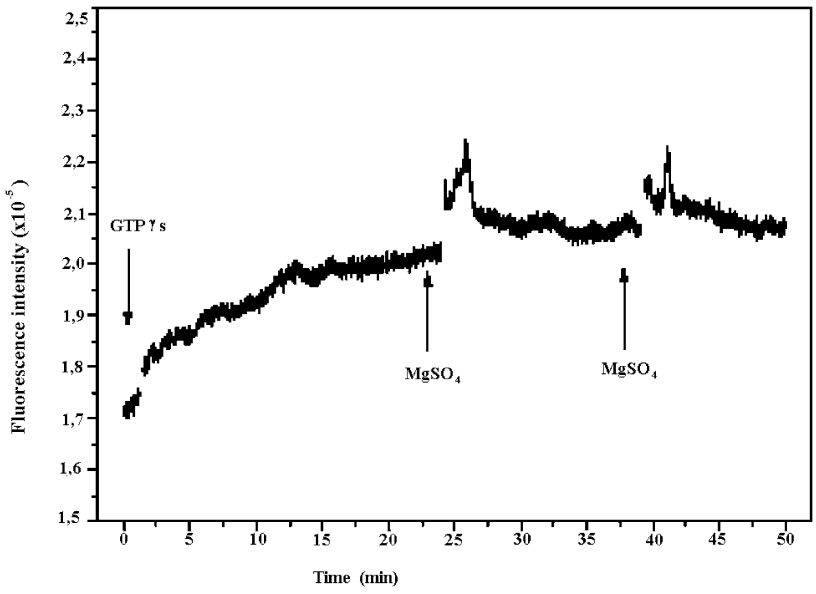

(A)

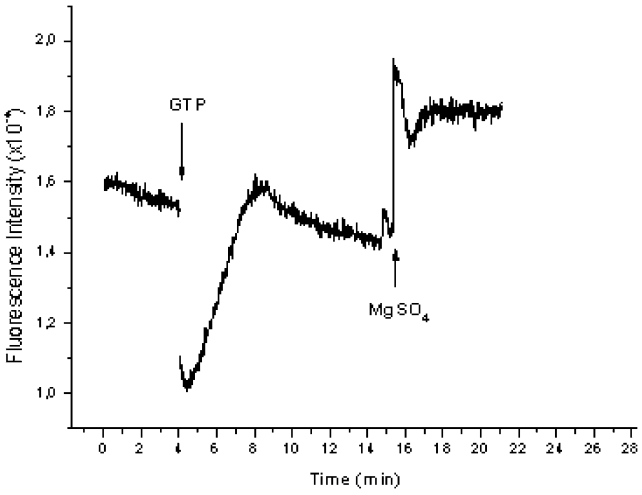

(B)

Fig. 2. The kinetics of GTP and GTPγS binding and GTP hydrolysis. (A) Effect of activation of the alpha subunit on the fluorescence of Goα. The fluorescence emission of Goα (400 nM) was measured in buffer A at 20°C. After 3 min, 1 μM GTPγS was added. At 23 and 38 min, $MgSO_4$ was added at 10 mM end concentration and incubation continued. (B) 200 nM of Goα protein in buffer A was placed in the spectrophotometer and the intrinsic fluorescence intensity was measured by stirring continuously. After 4 min, 10 μM GTP was added and recording was continued for 12 min. Subsequently, the sample was supplemented with 10 mM $MgSO_4$ and recording was performed for an additional 6 min. (C) The effect of GDP on the GTP induced change in Goα fluorescence. 200 nM of Goα was incubated as described above in buffer A containing 10 mM $MgSO_4$. After 4 min, 1 μM GTP was added to the cuvette, followed by the addition, after another 8 min, of 10 μM GDP.

higher than the GDP-bound form of the protein. On the other hand, when excess GDP was added to GTP-bound Goα, fluorescence intensity decayed to the initial, GDP-bound state of the protein (Fig. 2(C)).

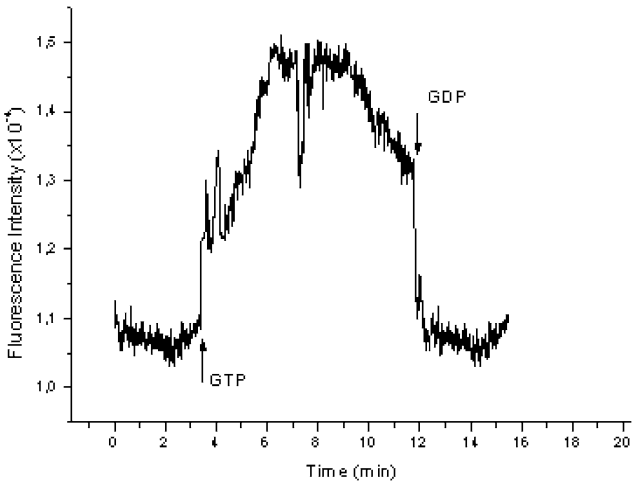

(C)

Fig. 2. (Continued.)

3.4. BODIPY-GTP analogs as a tool to measure real-time nucleotide binding

The fluorescence of the BODIPY group increases appreciably upon binding to some G proteins. This results from the specific association of the G protein with GTPγS and the movement of the guanine base from the BODIPY group [28]. We therefore performed the fluorescence-based, real time GTPγS binding assay to verify Goα protein activity. Emission maximum was found to be at 510 nm, as expected (Fig. 3(A)). A 30% increase in fluorescence peak intensity was observed upon addition of Goα and this signal was reduced by incubation with GTPγS for 20 min. To determine the interaction kinetics, the fluorescence of 50 mM BODIPY-GTPγS was measured for 2 min. After the addition of 400 nM Goα, the fluorescence gradually increased with time and reached a maximum at 35 min to a value 8% higher than the baseline. At the end of this period, 20 μM GTPγS was added and incubation was extended for an additional 30 min, after which the fluorescence decreased gradually (Fig. 3(B)).

3.5. FTIR

The ATR–FTIR spectroscopic technique is based on the measurement of IR radiation reflectance from the sample and therefore enables direct and rapid spectral acquisition, regardless of the thickness of the sample. Figure 4(A) shows ATR–FTIR spectrum of the protein at room temperature (20°C) in the 1700–1600 cm^{-1} region. This corresponds to the well characterized Amide I band, which arises principally from the C=O stretching vibration (80%) of the peptide bonds [17]. The Amide I band typically contains several unresolved secondary structural elements which can be resolved and easily seen in the second derivative spectrum of the protein (Fig. 4(B)). As seen from the figure, the band located at 1653 cm^{-1} is assigned to an α-helix, the band at 1632 cm^{-1} is assigned to a β-sheet, and the minor band at 1678 cm^{-1} is likely to arise from a β-turn. An anti-parallel β-sheet structure can be identified by the presence of another band near 1670–1695 cm^{-1}. This component is normally weak and its precise assignment is difficult by the overlap of absorptions from β-turns and unordered structures [17]. The band located at 1639 cm^{-1} is assigned to random coil and a tyrosine side chain is observed at 1617 cm^{-1}. The comparison of the intensity values of the subbands in the second derivative of the absorbance spectrum of

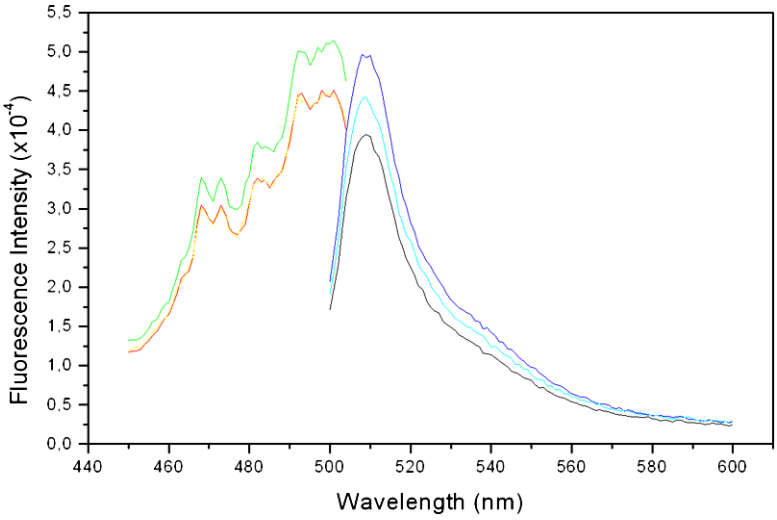

(A)

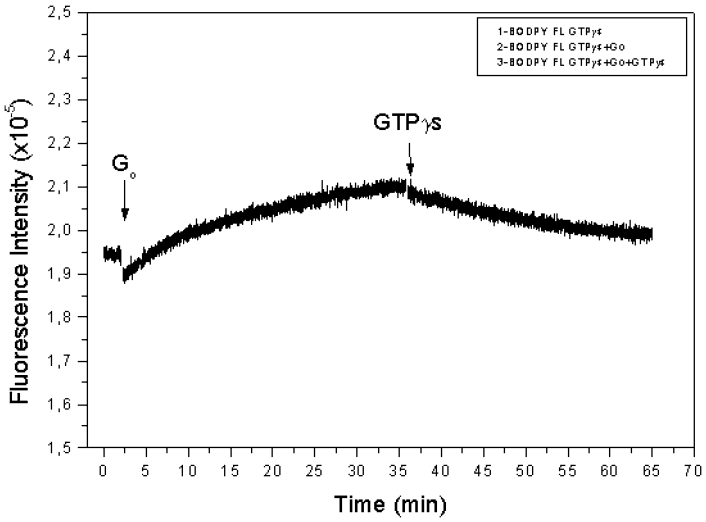

(B)

Fig. 3. Measurements with BODIPY FL-GTPγS. (A) emission spectra: BODIPY FL-GTPγS (black), BODIPY FL-GTPγ + Goα (400 nM) (navy), BODIPY FL-GTPγS + Goα (400 nM) + 1 μM GTPγS (turquoise), excitation spectra: BODIPY FL-GTPγS (red), BODIPY FL-GTPγ + Goα (400 nM) (green), BODIPY FL-GTPγS + Goα (400 nM) + 1 μM GTPγS (yellow). (B) Fluorescence measurements of BODIPY FL-GTPγS. The fluorescence of 50 nM BODIPY FL-GTPγS was measured at 20°C with λ_{ex} of 470 nm and λ_{em} of 510 nm for 2 min. 400 nM Goα was added and the change in fluorescence was followed for 35 min. Subsequently, GTPγS was added to give a final concentration of 20 μM and measurements were continued for an additional 35 min. (The colors are visible in the online version of the article; http://dx.doi.org/10.3233/ SPE-2011-0543.)

the protein clearly shows that the dominant secondary structure is α-helix. For the precise determination of the secondary structure content, NN approach was applied to the Amide I absorbance band as reported in Severcan et al. [41], which revealed the prediction as 42.3% α-helix, 13.4% β-sheet and 24.3% β-turn.

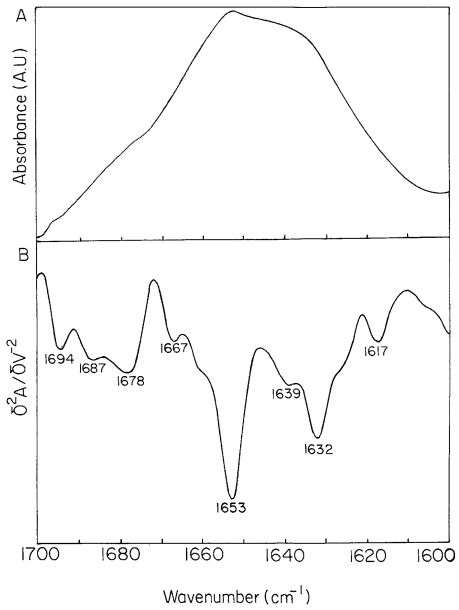

Fig. 4. FTIR spectroscopy of recombinant Goα. Pure Goα obtained after Mono Q chromatography was dialyzed against PBS and supplemented with 50 μM GDP. Goα (5 mg/ml) in PBS buffer was placed in a Spectrum 100 Spectrometer. Data acquisition and determination of secondary structure based on FTIR data are described under Section 2.

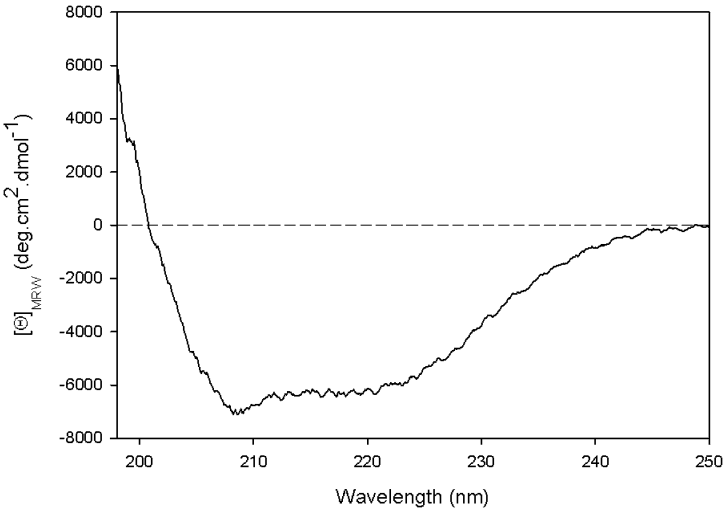

Fig. 5. Circular dichroism measurements of recombinant Goα. Pure Goα obtained after Mono Q chromatography was dialyzed against PBS and supplemented with 50 μM GDP. CD measurements in the far UV region were obtained as described under Section 2.

3.6. Circular dichroism

The far UV CD spectrum of Goα is displayed in Fig. 5. A qualitative analysis indicates that the spectrum is dominated by the contribution of α-helices, with negative bands at ∼222 and ∼208 nm, which was confirmed by deconvolution using the programs CONTIN, CDSSTR, SELCON and K2d

(see Section 2). This procedure revealed a helical content of ∼38%, with values of ∼15%, ∼17% and ∼30% for the strands, turns and unordered structures, respectively.

3.7. *Homology modeling of Goα (bovine)*

Because Goα-mouse and Goα-bovine sequences have a similarity higher than 97%, the structural features of Goα-bovine (theoretical model) were verified by data from the tertiary structure of Goα-mouse [PDB ID: 3c7k–Chain C] (experimental model) using the Swiss PDBViewer [16]. The modeled structure shows a secondary structural content of 38% α-helix and 13% β-sheet, which is closely similar with the secondary structure of the Goα-mouse, reported as 39% α-helix and 13% β-sheet. However, we found a difference in the region encompassing residues 115–121, which is located in the helical domain and join helices αB and αC. 50 loop models were created and refined by MODELLER for this region and the loop model which fit the energy considerations best was chosen. The *rmsd* values, calculated by Swiss PDBViewer [16], for all atoms and αB–αC loop of Goα-bovine obtained by homology modeling and those of Goα-mouse are 1.48 and 3.97 Å, respectively (Fig. 6(A)). Even though further structural refinement of this loop is required for meaningful predictions, our results strongly enforce the recent report speculating on the specific role of this region in effector coupling [43]. It is proposed that T117, which is located in this loop, is involved in mouse RGS16 recognition. To verify our model, we used HADDOCK program [9,10] for docking (Fig. 6(B)) the interacting portion of RGS16 (residues 164–172) to our modeled Goα. We found a similar interaction between bovine Goα and RGS16. Our model predicts an interaction of bovine Goα T117 with K 172, of RGS16, instead of T117 and K164 interaction in mouse.

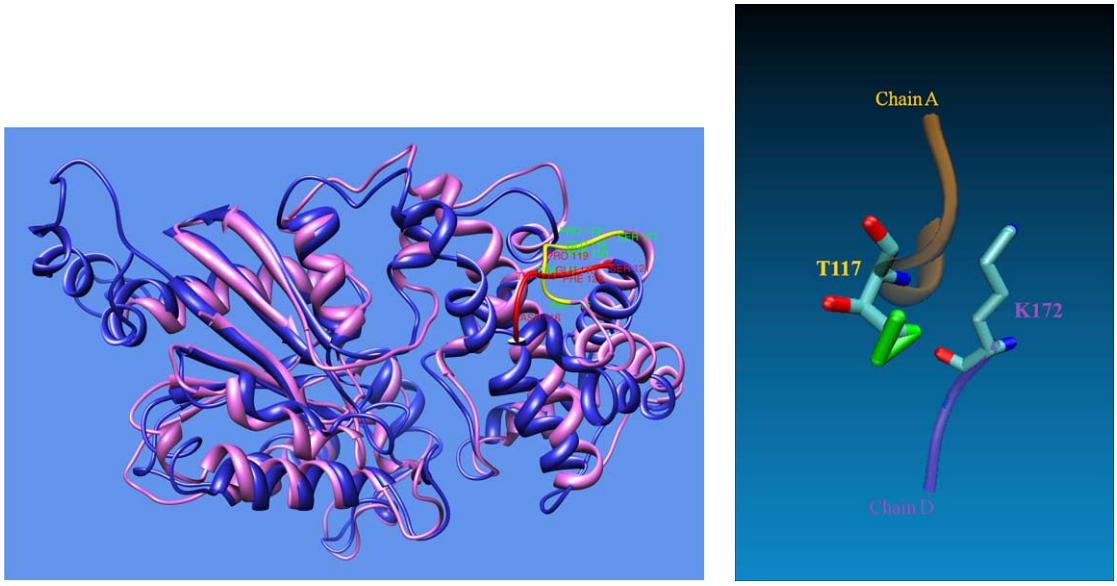

(A) (B)

Fig. 6. Models of Goα. (A) Superposition of theoretical Goα-bovine (in magenta) and experimental Goα-mouse (in pink) models. Loop regions of Goα-bovine and Goα-mouse spanning the nucleotides of 116–121 are shown in red and yellow, respectively. (B) Interaction of docked Goα bovine and Goα mouse (3ck7-D). (The colors are visible in the online version of the article; http://dx.doi.org/10.3233/SPE-2011-0543.)

4. Discussion

In this study we have modified previously reported purification schemes for heterotrimeric G-proteins in order to obtain a higher yield and activity of Goα in *E. coli*. We have also conducted preliminary structural studies to investigate the properties of Goα protein in solution. Because *E. coli* cells do not express heterotrimeric G protein subunits, recombinant Gα subunits can be purified to homogeneity, free of contaminating endogenous G proteins. On the other hand, there are also disadvantages of expressing recombinant Gα subunits in *E. coli* such as low activity and misfolded protein products due to the deficiency of post-translational mechanisms.

Goα amplified from pT7/NdeI/Goα template was subcloned into the pQE-80 vector system and expressed in *E. coli* Top10 cells. Prior to pQE-80, we also tested pTrcHis, pGEX-4T2, pET-28a vector systems to obtain optimum yields of soluble Goα under different growth and induction conditions. Among these, the pGEX-4T2 construct provided the highest expression yields but most of the protein was in the insoluble fraction as inclusion bodies (C. Nacar, O. Orun and B. Kan, unpublished data). The pQE-80 series vectors provide high translation rates and are therefore found to be the most effective system in terms of solubility. Our purification scheme consisted of Ni-NTA affinity chromatography, followed by Sephadex G-100 gel filtration and Mono Q chromatography. Using this simpler purification scheme, our yield was in close proximity to previously reported purification yields; furthermore, [^{35}S] GTPγS binding activity and GTP hydrolysis were in agreement with the literature.

We used different approaches to characterize the purified protein. Fluorescence techniques are becoming more widely used with real-time measurements. Therefore, we studied the kinetics of binding and hydrolysis by intrinsic fluorescence and BODIPY fluorophore tags. We first examined the intrinsic fluorescence properties of the protein. The wavelength for peak fluorescence intensity of Goα protein was 346 nm. It is known that ligands which activate G proteins induce a conformational change that can be detected by measurement of the intensity of fluorescence emission by tryptophan residues. Upon the interaction of the nonhydrolyzable analog of GTP, GTPγS, with Goα one observes an increase in the fluorescence intensity of the tryptophan residues as compared to that of the GDP-containing form of the protein. Higashijima et al. have demonstrated that the time course of this change reflects precisely the rate of association of GTPγS with the protein and is limited by the dissociation of GDP [21]. If Mg^{2+} is added subsequently, a rapid conformational change in the G protein produces a further increase of fluorescence intensity. It has been hypothesized that the more highly fluorescent state of Goα represents the activated state of the protein [21]. We observed a 20% increment in peak fluorescence intensity of recombinant Goα in the presence of GTPγS. This increase was 31% when $MgSO_4$ was added with GTPγS, thus confirming the active state of the recombinant protein. The binding rate of Goα for GTPγS in the absence of Mg^{2+} was found to be 0.36 min^{-1} and the rate for GTP hydrolysis was 2.4 min^{-1}, in agreement with values calculated by Higashijima et al. [21]. The same formation rate was also obtained with the BODIPY probe. These analyses were used to verify the correct conformational folding and activity of recombinant Goα protein.

Protein structure in solution reveals the native form of protein, thereby gives a more realistic picture of the protein. Both FTIR [14,19] and CD [25,27] are well established spectroscopic techniques for the study of biomacromolecular structure in solution. Therefore, these techniques are successfully applied for protein function studies. The success of protein secondary structure prediction by these low resolution spectroscopic techniques is strongly dependent on the methods that are developed. For example, neural networks based on Amide I band located between 1700 and 1660 cm^{-1} in infrared spectroscopy offers new computational approach that has served as a reliable alternative method for predicting protein

secondary structure in recent years [19,20,40,41]. This approach has been also successfully applied to proteins of biological tissues and membranes [1,2,12].

Advances in deconvolution methods for CD [15,44,48] spectra, in particular, have improved significantly the reliability of this technique to calculate protein secondary structure content. We used these approaches to analyze the secondary structure of recombinant Goα. As expected, Goα exhibited a high resemblance to Giα, lending further support to correct expression and folding of recombinant Goα protein. With Goα, FTIR and CD analyses gave similar values for both the α-helical (42 and 38%, respectively) and β-strand (13 and 15%, respectively) content. These values are in remarkable agreement with those calculated for both the modeled structure (38 and 13% for helices and strands, respectively) and the mouse Goα X-ray structure [43].

Theoretical methods are being widely used in predictions of protein structure and function because of the limitations of experimental studies such as cost, time and infrastructure, and big advances in computational capabilities in recent years. The secondary structure predicted by homology modeling [30] was obtained before the Goα-mouse crystal structure was released and is in very good agreement with the crystal structure [43], except for the loop between αB and αC helices of the helical domain. The sequence dissimilarity of αB–αC loops of Go and Gi proteins makes this loop a possible candidate for interaction with other partners [43]. As reported by this recent study, one of the interaction determinants between Goα and RGS16 is the Lys-164 of RGS16 and Thr-117 of Goα that lies on αB–αC loop. The difference between the loop structures of our model and the 3c7k: Chain-C (rmsd value of 3.97 Å) may arise from the reported mobility (indicated by the elevated temperature factors of atoms in the 3c7k: Chain-C) of the loop [43]. Because this mobility is an obstacle in determining the tertiary structure of the loop, theoretical models may be valuable for predicting possible functions of this region. Moreover, further refinement of the model of Goα in complex with effectors using docking approaches would provide the required assessment of details in structure responsible for its specificity. To this end, we docked our modeled Goα with mouse RGS16 and found that interactions established in mouse are conserved in our docked model for bovine as well. The only difference came from the flexible loop of bovine Goα interaction with RGS 16. In our model T117 interacted with K172 as opposed to T117 and K164 interaction in mouse. The differences revealed by docking studies using RGS16 give additional insights for the putative roles of the αB–αC loop in interactions with other molecules, such as guanine nucleotide exchange factors (GEFs), GTPase accelerating proteins (GAPs) and effectors.

In conclusion, we hereby present practical and efficient methods to purify and characterize Goα. We also demonstrate how different approaches can be combined to predict the structural determinants of a protein. The secondary structure content of the protein in solution predicted by FTIR and CD spectroscopy were found to be in agreement with those calculated by homology modeling and the mouse Goα X-ray structure [43]. Our results indicate that Goα, when expressed in the above mentioned conditions, can be easily purified in sufficient amounts for biochemical studies. Furthermore, we confirm that Goα, in solution, exhibits a high similarity to other heterotrimeric G-proteins in structure, except for some domains that possibly take part in interaction of Goα with other proteins. Our homology model also confirms the importance of the αB–αC loop in rendering specificity for protein-protein interactions.

Acknowledgements

The authors thank Drs Sule Oncul and Stephen Martin for a help in fluorescence spectroscopy and CD spectra analysis, respectively, and Engin Yapici for technical help in collecting FTIR spectra. We

also thank Dr. Zehra Sayers from Sabanci University and Dr. Katherine Brown from Imperial College for their valuable suggestions on cloning and purification.

Funding

This work was supported by grants Marmara University Research Fund (SAG-DKR-100105-0003 and SAG-BGS-120707-0136) and in part by grants from the Fonds de la Recherche Fondamentale et Collective (contract numbers 2.4550.05 and 2.4530.09) and by the Belgian program of Interuniversity Attraction Poles initiated by the Federal Office for Scientific Technical and Cultural Affaires (PAI n° P6/19). A.M. was Research Associate (1998-2010) of the National Fund for Scientific Research (F.R.S.-FNRS, Belgium).

References

[1] O. Bozkurt, M. Severcan and F. Severcan, Diabetes induces compositional, structural and functional alterations on rat skeletal soleus muscle revealed by FTIR spectroscopy: a comparative study with EDL muscle, *Analyst* **135** (2010), 3110.
[2] G. Cakmak, F. Zorlu and F. Severcan, Screening of restoring effect of amifostine on radiation induced structural and functional variations in rat liver microsomal membranes by FTIR spectroscopy, *Anal. Chem.* **83** (2011), 2438.
[3] Y. Cao and Y. Huang, Palmitoylation regulates GDP/GTP exchange of G protein by affecting the GTP-binding activity of Goα, *Int. J. Biochem. Cell Biol.* **37** (2005), 637.
[4] L.T. Chen, A.G. Gilman and T. Kozasa, A candidate target for G protein action in brain, *J. Biol. Chem.* **274** (1999), 26931.
[5] D.E. Clapham and E.J. Neer, G protein beta gamma-subunits, *Annu. Rev. Pharmacol. Toxicol.* **37** (1997), 167.
[6] D.E. Coleman and S.R. Sprang, Crystal structures of the G protein $G_{i\alpha 1}$ complexed with GDP and Mg^{2+}: a crystallographic titration experiment, *Biochemistry* **37** (1998), 14376.
[7] D.E. Coleman and S.R. Sprang, Structure of $G_{i\alpha 1}$.GppNHp, autoinhibition in a G_α protein-substrate complex, *J. Biol. Chem.* **274** (1999), 16669.
[8] R. Collu, C. Bouvier, G. Lagacé, C.G. Unson, G. Milligan, P. Goldsmith and A.M. Spiegel, Selective deficiency of guanine nucleotide-binding protein Go in two dopamine-resistant pituitary tumors, *Endocrinology* **122** (1988), 1176.
[9] S.J. de Vries, A.D.J. van Dijk, M. Krzeminski, M. van Dijk, A. Thureau, V. Hsu, T. Wassenaar and A.M.J.J. Bonvin, HADDOCK versus HADDOCK: new features and performance of HADDOCK2.0 on the CAPRI targets, *Proteins* **69** (2007), 726.
[10] C. Dominguez, R. Boelens and A.M.J.J. Bonvin, HADDOCK: a protein–protein docking approach based on biochemical or biophysical information, *J. Am. Chem. Soc.* **125** (2003), 1731.
[11] A. Fiser, R.K. Do and A. Sali, Modeling of loops in protein structures, *Protein Sci.* **9** (2000), 1753.
[12] S. Garip, E. Yapici, N.S. Ozek, M. Severcan and F. Severcan, Evaluation and discrimination of simvastatin-induced structural alterations in proteins of different rat tissues by FTIR spectroscopy and neural network analysis, *Analyst* **135** (2010), 3233.
[13] A.G. Gilman, G proteins: transducers of receptor-generated signals, *Annu. Rev. Biochem.* **56** (1987), 615.
[14] E. Goormaghtigh, J.M. Ruysschaert and V. Raussens, Evaluation of the information content in infrared spectra for protein secondary structure determination, *Biophys. J.* **90** (2006), 2946.
[15] N. Greenfield, Using circular dichroism spectra to estimate protein secondary structure, *Nat. Protoc.* **1** (2007), 2876.
[16] N. Guex and M.C. Peitsch, SWISS-MODEL and the Swiss-PdbViewer: an environment for comparative protein modeling, *Electrophoresis* **18** (1997), 2714.
[17] P. Haris and F. Severcan, FTIR spectroscopic characterization of protein structure in aqueous and non-aqueous media, *J. Molecular Catalysis B: Enzymatic* **7** (1999), 207.
[18] J.R. Hepler and A.G. Gilman, G proteins, *Trends Biochem. Sci.* **17** (1992), 383.
[19] J.A. Hering, P.R. Innocent and P.I. Haris, An alternative method for rapid quantification of protein secondary structure from FTIR spectra using neural networks, *Spectrosc. Int. J.* **16** (2002), 53.
[20] J.A. Hering, P.R. Innocent and P.I. Haris, Towards developing a protein infrared spectra databank (PISD) for preotomics research, *Proteomics* **4** (2004), 2310.
[21] T. Higashijima, K.M. Ferguson, P.C. Sternweis, E.M. Ross, M.D. Smigel and A.G. Gilman, The effect of activating ligands on the intrinsic fluorescence of guanine nucleotide-binding regulatory proteins, *J. Biol. Chem.* **262** (1987), 752.

[22] W. Humphrey, A. Dalke and K. Schulten, VMD: visual molecular dynamics, *J. Mol. Graph.* **14** (1996), 33.
[23] J.M. Justice, M. Bliziotes, L.A. Stevens, J. Moss and M. Vaughan, Involvement of N-myristoylation in monoclonal antibody recognition sites on chimeric G protein α subunits, *J. Biol. Chem.* **270** (1995), 6436.
[24] K. Kato, T. Asano, N. Kamiya, H. Haimoto, S. Hosoda, A. Nagasaka, Y. Ariyoshi and Y. Ishiguro, Production of the α-subunit of guanine nucleotide-binding G-protein Go by neuroendocrine tumors, *Cancer Res.* **47** (1987), 5800.
[25] S.M. Kelly, T.J. Jess and N.C. Price, How to study proteins by circular dichroism, *Biochim. Biophys. Acta* **175** (2005), 119.
[26] M.A. Larkin, G. Blackshields, N.P. Brown, R. Chenna, P.A. McGettigan, H. McWilliam, F. Valentin, I.M. Wallace, A. Wilm, R. Lopez, J.D. Thompson, T.J. Gibson and D.G. Higgins, Clustal W and Clustal X version 2.0, *Bioinformatics* **23** (2007), 2947.
[27] S.R. Martin and M.J. Schilstra, Circular dichroism and its application to the study of biomolecules, *Methods Cell Biol.* **84** (2008), 263.
[28] D.P. McEwen, K.R. Gee, H.C. Kang and R.R. Neubig, Fluorescent BODIPY-GTP analogs: real time measurement of nucleotide binding to G proteins, *Anal. Biochem.* **291** (2001), 109.
[29] D.P. McEwen, K.R. Gee, H.C. Kang and R.R. Neubig, Fluorescence approaches to study G protein mechanisms, *Methods Enzymol.* **344** (2002), 403.
[30] C. Nacar, Studies on the tertiary structure of the alpha subunit of Go protein by experimental and theoretical methods, PhD thesis, Marmara University, Istanbul, Turkey, 2007.
[31] H. Nakata and T. Kozasa, Functional characterization of Goα signaling through G protein-regulated inducer of neurite outgrowth 1, *Mol. Pharmacol.* **67** (2005), 695.
[32] I. Nishimoto, T. Okamoto, Y. Matsuura, S. Takahashi, T. Okamoto, Y. Murayama and E. Ogata, Alzheimer amyloid protein precursor complexes with brain GTP-binding protein Go, *Nature* **362** (1993), 75.
[33] S. Offermanns and M.I. Simon, Organization of transmembrane signaling by heterotrimeric G proteins, in: *Cancer Surveys*, J. Tooze, P.J. Parker and T. Pawson, eds, Cold Spring Harbor Laboratory Press, New York, 1996, p. 177.
[34] C.N. Pace, F. Vajdos, L. Fee, G. Grimsley and T. Gray, How to measure and predict the molar absorption coefficient of a protein, *Protein Sci.* **4** (1995), 2411.
[35] E.F. Pai, U. Krengel, G.A. Petsko, R.S. Goody, W. Kabsch and A. Wittinghofer, Refined crystal structure of the triphosphate conformation of H-ras p21 at 1.35 Å resolution: implications for the mechanism of GTP hydrolysis, *EMBO J.* **9** (1990), 2351.
[36] E.F. Pettersen, T.D. Goddard, C.C. Huang, G.S. Couch, D.M. Greenblatt, E.C. Meng and T.E. Ferrin, UCSF chimera – a visualization system for exploratory research and analysis, *J. Comput. Chem.* **13** (2004), 1605.
[37] J.C. Phillips, R. Braun, W. Wang, J. Gumbart, E. Tajkhorshid, E. Villa, C. Chipot, R.D. Skeel, L. Kalé and K. Schulten, Scalable molecular dynamics with NAMD, *J. Comput. Chem.* **26** (2005), 1781.
[38] A.M. Preininger and H.E. Hamm, G protein signaling: insights from new structures, *Sci. STKE* **2004** (2004), re 3.
[39] A. Sali and T.L. Blundell, Comparative protein modelling by satisfaction of spatial restraints, *J. Mol. Biol.* **234** (1993), 779.
[40] M. Severcan, F. Severcan and I.P. Haris, Estimation of protein secondary structure from FTIR spectra using neural networks, *J. Mol. Struct.* **565–566** (2001), 383.
[41] M. Severcan, F. Severcan and P.I. Haris, Using artificially generated spectral data to improve protein secondary structure prediction from FTIR spectra of proteins, *Anal. Biochem.* **332** (2004), 238.
[42] M.I. Simon, M.P. Strathmann and N. Gautam, Diversity of G proteins in signal transduction, *Science* **252** (1991), 802.
[43] K.C. Slep, M.A. Kercher, T. Wieland, C.-K. Chen, M.I. Simon and P.B. Sigler, Molecular architecture of Gαo and the structural basis for RGS16-mediated deactivation, *Proc. Natl. Acad. Sci. USA* **105** (2008), 6243.
[44] N. Sreerama and R.W. Woody, Estimation of protein secondary structure from circular dichroism spectra: comparison of CONTIN, SELCON, and CDSSTR methods with an expanded reference set, *Anal. Biochem.* **287** (2000), 252.
[45] P.C. Sternweiss and J.D. Robishaw, Isolation of two proteins with high affinity for guanine nucleotides from membranes of bovine brain, *J. Biol. Chem.* **259** (1984), 13806.
[46] N. Vardi, Alpha subunit of Go localizes in the dendritic tips of ON bipolar cells, *J. Comp. Neurol.* **395** (1998), 43.
[47] N. Wettschureck and S. Offermanns, Mammalian G proteins and their cell type specific functions, *Physiol. Rev.* **85** (2005), 1159.
[48] L. Whitmore and B.A. Wallace, DICHROWEB, an online server for protein secondary structure analyses from circular dichroism spectroscopic data, *Nucleic Acids Res.* **32** (2004), W668.
[49] L. Whitmore and B.A. Wallace, Protein secondary structure analyses from circular dichroism spectroscopy: methods and reference databases, *Biopolymers* **89** (2008), 392.